Structural opto-mechanical model of AZIMOV

The deployable telescope for CubeSat

J.-F. Sauvage, N. Schwartz, L. Buron, A. Zeshan, M. Dumont, et al.

Published version information:

Citation: J Sauvage et al. Structural opto-mechanical model of AZIMOV, the deployable telescope for CubeSat. In Space Telescopes and Instrumentation 2022: Optical, Infrared, and Millimeter Wave, Montréal, Canada, 17-23 Jul 2022, (2021): 8.

DOI: 10.1117/12.2629844

PROCEEDINGS OF SPIE

SPIEDigitalLibrary.org/conference-proceedings-of-spie

Structural opto-mechanical model of AZIMOV: the deployable telescope for CubeSat

J.-F. Sauvage, N. Schwartz, L. Buron, A. Zeshan, M. Dumont, et al.

J.-F. Sauvage, N. Schwartz, L. Buron, A. Zeshan, M. Dumont, M. Ferrari, J. Petit, P. Vola, M. Jaquet, T. Pamplona, B. Rosier, A. Miniussi, V. Michau, "Structural opto-mechanical model of AZIMOV: the deployable telescope for CubeSat," Proc. SPIE 12180, Space Telescopes and Instrumentation 2022: Optical, Infrared, and Millimeter Wave, 121800B (27 August 2022); doi: 10.1117/12.2629844

SPIE.

Event: SPIE Astronomical Telescopes + Instrumentation, 2022, Montréal, Québec, Canada

Structural opto-mechanical model of AZIMOV The deployable telescope for CubeSat

J.-F. Sauvage[a,b], N. Schwartz[c], Lucie Buron[b], A. Zeshan[c], M. Dumont[a,d], M. Ferrari[b], J. Petit[e], P. Vola, M. Jaquet, T. Pamplona, B. Rosier[e], A. Miniussi[e], V. Michau[e]
[a]ONERA, DOTA, F-13661 Salon Cedex Air – France; [b]Aix Marseille Univ, CNRS, CNES, LAM, Marseille, France;
[c]UK Astronomy Technology Centre, Blackford Hill, Edinburgh EH9 3HJ, United Kingdom;
[d]INESTEC, FEUP, Porto, Portugal; [e]ONERA, DOTA, Palaiseau - France

ABSTRACT

Today, the combination of high angular resolution and high revisit rate is not readily available from space, at least not at a reasonable cost. Many applications in the science, civil or defense domains would benefit from having access to detailed images of the ground as often as possible, in order to study temporal evolutions of specific events. The high angular resolution requires large optics hence large platforms, whereas the revisit rate requires constellations of multiple satellites and therefore small and affordable platforms. We proposed the concept of a deployable telescope onboard a CubeSat, called AZIMOV [1, 3, 5], to address this specific gap. Reaching a diameter of 30 cm once deployed, this concept gives access to a meter resolution on the ground from a Low Earth Orbit, or to a 70 cm resolution on Mars surface from a 400 km polar orbit. We study in this paper the performance of such a telescope in the aggressive thermal environment of space, with respect to the tight optical requirements of the system.

Keywords: Space active optics, diffraction limit, Earth observation, phasing segmented telescope, CubeSat

1. INTRODUCTION

Today, images taken from space with high angular resolutions (typically better than a metre resolution) and high revisit rates (especially several times per day) are in high demand in many application areas.

One can highlight for instance the scientific study of climate that in particular requires measurement of Earth's Albedo at small scales several times per day (the albedo evolves during the day and depends on the position of the Sun). To date the Sentinel missions provide the best albedo measurements at a resolution of several tens of meters and at best at a frequency of once a day. Having detailed images combining both high spatial and temporal resolutions would provide crucial quantitative information to understand climate forcing at small scales around large urban areas. It will also provide guidance on the future urbanization of metropoles to make them more climate-friendly and resilience to climate change. In this aim, a constellation of 6 30 cm-telescopes in a sun-synchronous orbit centred on a specific metropole orientation (Paris-Turin axis for instance) would bring crucial information on this aspect.

In a separate field of science, one can highlight the interest of such a constellation for Mars exploration and analysis. A constellation of 4 to 6 satellites of 30cm-telescopes would be a game changer to understand the storms and cloud formation on Mars and globally for monitoring and forecasting Mars' weather. Such a constellation would in addition bring high value images for the identification of future mission landing sites. NASA identified both these objectives as priority for the exploration of Mars.

On top of these objectives, one can cite a high interest for civil applications (natural disaster detection and monitoring). A constellation of 6 AZIMOV would bring clear information every 6 to 4 hours on fire, flooding, oil disasters. One finally can add the obvious interest of defence applications, where the survey, strategic and operational aspects require metric resolution to estimate the number of vehicles (hence quantify the forces in presence), as well as acceptable revisit rates to be able to identify troop movements.

All these objectives require a constellation of 4 to 6 30cm telescope in orbit. The metric resolution can only be brought by an optical system at the limit of diffraction in the visible wavelength. This requires controlling the wavefront quality

Space Telescopes and Instrumentation 2022: Optical, Infrared, and Millimeter Wave, edited by Laura E. Coyle, Shuji Matsuura, Marshall D. Perrin, Proc. of SPIE Vol. 12180, 121800B · © 2022 SPIE · 0277-786X · doi: 10.1117/12.2629844

at a sufficient level, typically 40 nanometres of wavefront error [WFE] in an aggressive case, and up to 70-100 nm in a slightly relaxed scenario.

The concept of AZIMOV is a 30cm telescope in Low Earth Orbit [LEO]. In order to keep the cost of this system as low as possible, the use of the CubeSat standard is proposed, keeping the complete size of the satellite in a 6U range. A 30 cm monolithic aperture would require much a larger platform. We propose a folded M1 and M2 telescope that can fit into a 4U volume, and that can deploy the 30 cm full aperture once in orbit. This concept proposed by UK-ATC [ref] requires deploying a segmented primary mirror, a secondary mirror, and possibly baffles. Maintaining sufficient image quality during the operational lifetime of such a concept requires the measurement of the position of the segments and the control their position in space and in real-time.

The total acceptable wavefront error is set to 40 nm RMS (diffraction-limit in the visible), with many factors contributing to the wavefront quality degradation. We have listed them in Figure 1, with associated values for each of them. The decomposition was first proposed in [2] and here is provided with more detailed. The optical surface quality, their initial alignment, and the impact of launch on the optical alignment has to be quantified and fit within a restricted error budget to ensure the final optical quality. Of course, the capacity of the telescope to control a part of the wavefront is crucial to reaching the final performance, and all the terms in the table below are to be understood after active optics [AO] correction. In particular, the thermal gradient environment of the satellite in LEO will create varying piston, tip, and tilt [PTT] modes, moving the petal away from their ideal position. The amplitudes of these displacements still have to be studied. We want to focus in this paper on one specific term of this list, which is the inner petal deformation under thermal load. This particular term can be of large amplitude, will degrade the optical quality, and there is little that can be done to correct it (only PPT can be compensated).

Category	Definition	Error Source	Comment	Error #	WFE budget
Intrinsic optical errors	Quality of optics	Manufacturing	Low-order residual manufacturing error of the optics (mostly M1 and M2)	1	10
		Polishing	Polishing errors, mainly high-orders	2	30
	Initial alignment (on the ground)	Integration / alignment	The optical residual of the optics after alignment of the system in laboratory, excl. segment phasing residuals (e.g., lenses aligment, M1 positioning accuracy)	3	30
	Ground to space degradation (static or one-time events)	Launch impact	Degradation of the optical quality due to the launch (e.g. vibrations move optics / detectors arround)	4	10
		Space environment	Degradation of the optical quality due to the difference of environment between ground and space	5	10
	Observation environment (dynamic)	Thermal load	Varying thermal load will modify the optics and degrade the optical quality (e.g., shape of the M1 and M2 optics)	6	31
		Drift and jitter	Effect of the high-freq vibrations and LoS drift during integration	7	20.2
M1 deployable segments	Differential piston residual	Pist. Error between segments	Phasing residual between M1 segments, after active optics correction. Only tip, tilt, piston is controlled. Lateral X-Y movements are not, leading to additional WFE error.	8	20
	Differential tip-tilt residual	TT Error between segments	Orientation residual between M1 segments, after active optics correction.	9	20
	Scalloping [0]	Focus error between M1 and M2	Compensation of focus error with M1 (i.e. individual segments have wrong RoC).	10	10
	M1 deployment precision	M1 deployment error	Only tip, tilt, piston is controlled. Lateral X-Y movements are not, leading to additional WFE error.	10.1	0
M2 deployable segments	Secondary mirror deployment precision	M2 deployment error	Only tip, tilt, piston is controlled. Lateral X-Y movements are not, leading to additional WFE error.	11	0
	Tip-tilt residual	M2 control	Residual M2 tip-tilt error (rX, rY)	12	20
	Focus residual	M2 control	Residual M2 focusing error (Z)	13	20
Contingency	Other unaccounted errors	Misc.		14	10
					72

Figure 1: Error budget breakdown. The list of the contributors to the wavefront aberrations is given in left columns and is detailed by categories (intrinsic to the optics, related to the deployment of M1, of M2, and contingencies). The number associated to each term is given in nanometre RMS of wavefront over the full pupil. The total envelop is estimated at ~70 nm RMS.

We have established an acceptable level of 30 nm RMS for the wavefront error generated by the petal deformation under thermal environment. This term is to be understood over the full pupil of AZIMOV. It translates into a 100 nm PV maximum envelop for each petal.

2. STOP MODEL DEVELOPMENT

To analyse and better understand the behaviour of a single petal of AZIMOV, we need a triple model.

- From thermal environment to temperature map

    - The satellite, and hence the petals, are surrounded by a complex and evolving thermal environment. The Sun, Earth, space, and the satellite itself are heating sources that are creating a non-uniform temperature distribution on the surface of the M1 mirror and in the volume of the satellite. On top of this, their position in space is evolving along the orbit and creates time-evolving thermal gradients. The material chosen for the petal is important, in particular its emissivity, which condition the capacity of the material to reflect incoming light and heat fluxes.
- From temperature map to mechanical deformation
    - The temperature maps at the surface of the satellite are boundary conditions that translate into a mechanical deformation of the considered system after some time constant. Here the shape and choice of material are affecting this transformation.
- From mechanical deformation to wavefront error
    - The wavefront error is our final quality criterion. The previous models need to be converted into wavefront error to verify the compatibility with a diffraction-limited imager.

We have chosen to develop as simple a model as possible, to understand the physics behind them, and to apply them to a large number of configurations. Our first models analytical, then develop with simple excel solvers, and finally cross-validated with end-to-end industrial software (COMSOL, NASTRAN-PATRAN).

The first model represents the analytical dependence of the petal to the thermal gradient. The main deformation to be expected is a bending of the petal across its larger dimension. Figure 2 [left] shows the expected deformation with a full aluminium petal, under a 10°C temperature difference between the two faces. The decomposition of this deformation on the wavefront maps can be split between piston-tip-tilt modes and higher order modes (Figure 2 [right]). For a 10°C temperature difference, the amplitude of the first ones is around 10 micron, the amplitude of the second one is 14 micron (wavefront Pic-to-Valley). If the first contributor can be easily addressed by an AO system as specified in [5], the second one is completely killing the performance of the imager and cannot be corrected. Equation 1 shows a very simplified model of the single petal bending, as a parallelepiped volume of dimensions 10x10x1cm^3. The order of magnitude of the deformation expected is completely compatible with what is seen on NASTAN/PATRAN.

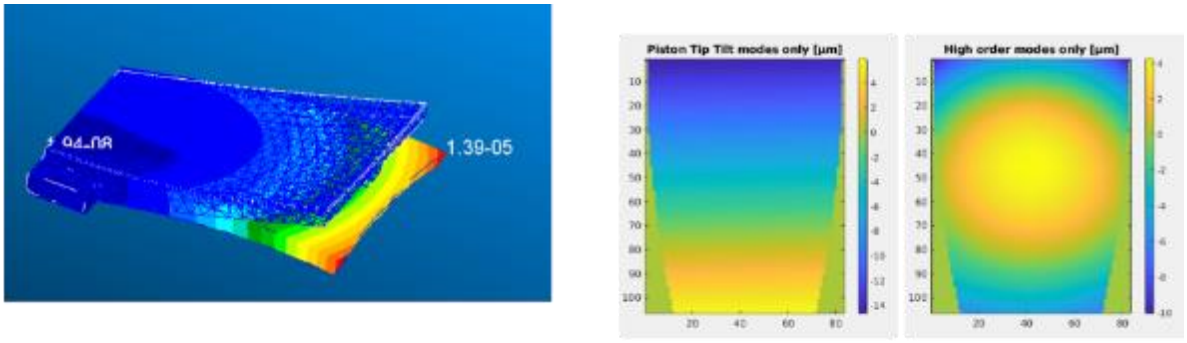

Figure 2: End-to-End deformation of a single petal due to temperature non-uniformity. [left] magnified visualization of the bending effect due to a temperature difference between the optical and back surface of the petal. [right] decomposition of the deformation on the wavefront in piston-tip-tilt and in high order of deformation. The temperature difference is 10°C, the material is aluminium.

Equation 1: analytic model of the bending amplitude, depending on the CTE (alpha), the size of petal (height H and length L) and the temperature difference between the optical and back surface Delta T.

Figure 3 shows the dependence of this bending effect on the temperature gradient along the petal width, depending on the material chosen. Different sets of material have been identified, for their diversity in CTE, conductivity, coupled to their capacity to be polished. The aluminium is the most sensitive to thermal gradient. In order to guarantee a 100 nm PV maximum deformation, a delta T has to be smaller than 0.07°C. Cordierite, on the opposite, can tolerate a much larger thermal gradient of close to 10°C.

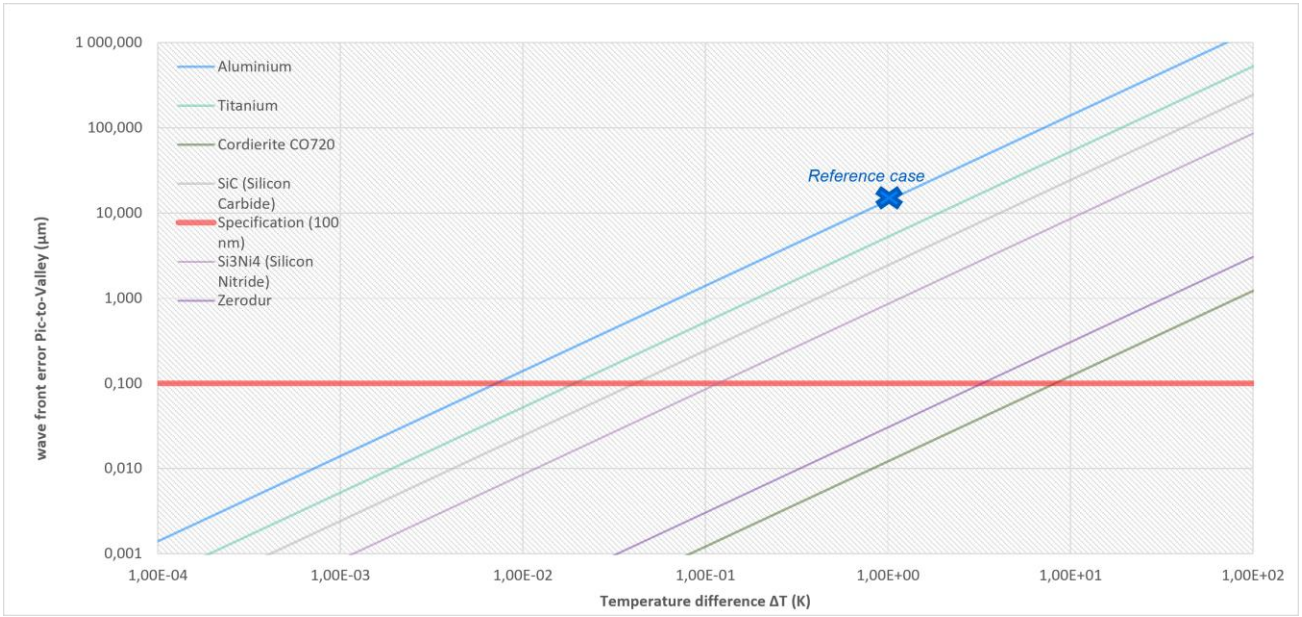

Figure 3: wavefront aberration created by a given temperature difference between the optical and back surface of the petal, depending on the material. A reference case has been validated by End-to-End simulation using Nastran.

This first model does not account for the photometric model, including the heating sources around the satellite. We are now considering this part of the model, considering the heat transfer between the Sun, Earth, space, with the petal. This model depends on the geometry of the petal, the view factors of each face, the conductivity of the material, and the position of the heating sources with respect to the petal. The petal is assimilated to a regular rectangle of 8 nodes. The heat balance Equation 2, derived from the first thermodynamic law, describes how the heat is absorbed by each node, either coming from external sources, or coming from the other nodes. This equation if written at the equilibrium in a first step (T does not depend on t) in order to get the temperature distribution after an infinite time. Of course, this case gives only an asymptotic description, which is not valid in orbit due to the relative short time (approx. 90 minutes) of the orbit with respect to the typical reaction time of the chosen material. The index *n* in this equation refers to the 8 nodes of the parallelepiped modelizing the petal, as shown in Figure 4.

$$0 = \Phi^n_{Sun} + \Phi^n_{Earth\ IR} + \Phi^n_{Albedo} + \lambda \sum_{i=1}^{8} S_{ni}\ \frac{(T_n - T_i)}{l_{ni}} - \sigma \epsilon S T_n^4$$

Equation 2: heat balance equation at equilibrium (left term is zero), depending on the flux absorbed by the petal (three first terms), the conduction flux between the petal nodes, and the flux emitted by the petal.

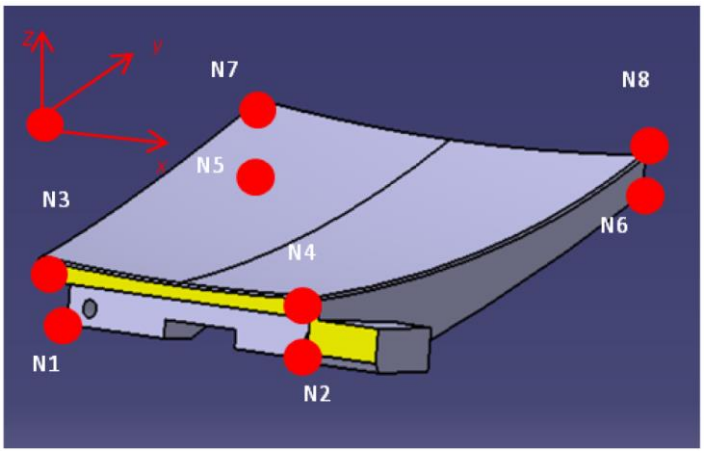

Figure 4: simplified model of the petal, used in this paper to perform the STOP analysis. The petal is simplified as a regular parallelepiped, and modified as 8 nodes and 6 surfaces.

Figure 5 gathers the two previous models and gives the wavefront aberration effectively generated in orbit. Two extreme situations have been considered: the satellite is in between the Sun and the Earth, and the Sun is eclipsed by Earth. In the first situation, the back surface of the petal becomes warmer than the front one, and the petal bends toward the Earth. In the second case, the back surface becomes colder and the petal bends toward the outer space. The first situation shows that Titanium and Silicon Carbide are not acceptable and produce a too large deformation to the wavefront, where the other materials are acceptable, including aluminium. In the second situation, all the gradients are much smaller due to the fainter heat source represented by the Earth. Nonetheless, in these two situations the bending is opposite. The effect of the wavefront is therefore cumulated between the first and second situation.

An important aspect of this analysis is to understand the impact of the material choice on how the petal deforms. Off course an output is to identify a valuable material. We have chosen 6 materials listed in Tableau 1 below, for their very different characteristic in term of conductivity and CTE. They have been chosen as well for their compatibility with polishing. The petals of AZIMOV are made of a single material and polished.

	Cordierite	Zerodur	Aluminium	Silicon Nitride (Si3Ni4)	Titanium	Silicon Carbide (SiC)
Conductivity $(W.m^{-1}.K^{-1})$	3	1	204	10	20	3.8
Specific Heat $(J.K^{-1}.kg^{-1})$	1465	800	896	750	520	510

	Cordierite	Zerodur	Aluminium	Silicon Nitride (Si3Ni4)	Titanium	Silicon Carbide (SiC)
CTE $(\times 10^{-6})$ $(m/m/K)$	0.02	0.05	23.00	1.40	8.60	4.00

Tableau 1: list of 6 material chosen for this work.

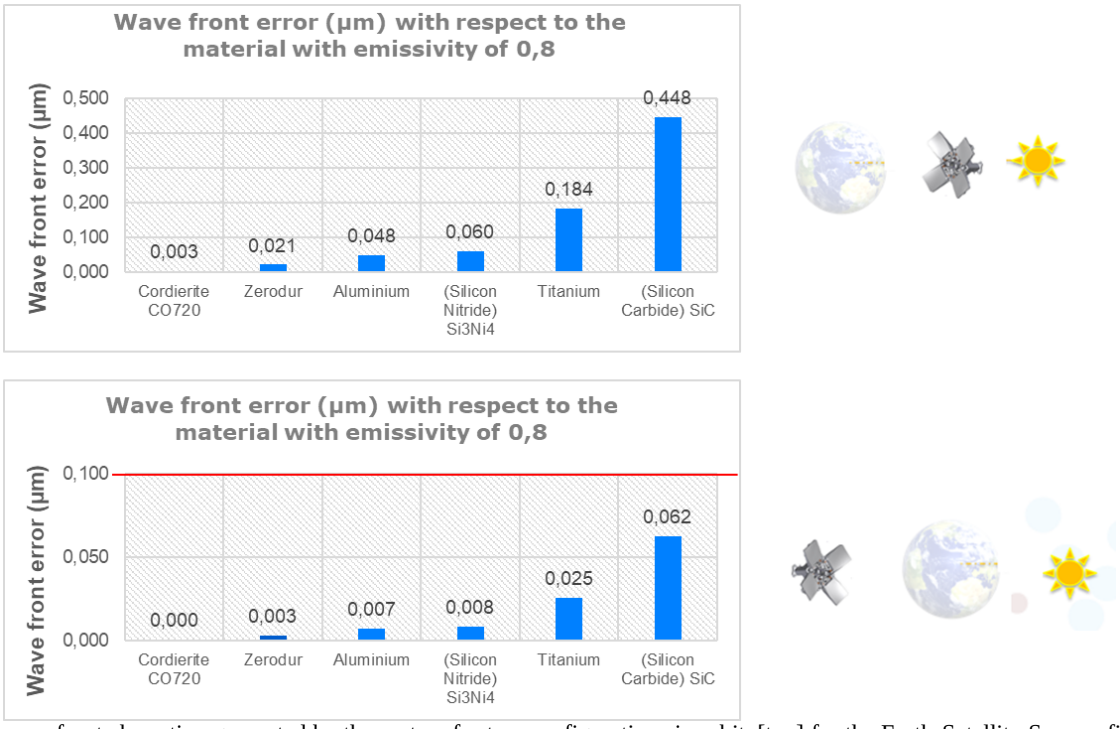

Figure 5: wavefront aberration generated by the system for two configurations in orbit. [top] for the Earth-Satellite-Sun configuration. The temperature gradient is the highest, and the wavefront error as well. [bottom] for the Satellite-Earth-Sun configuration. The deformation is opposite, and much smaller.

This result depends on a crucial parameter, which is the rugosity of the material (characterized by the emissivity). The more polished are the surface, the more they reflect the heating sources, the less they absorb, the smaller the temperature gradients, and finally the smaller the wavefront aberrations. The naturally polished surface (facing the Earth) is chosen with an emissivity of 0.05. An emissivity of 0.5 chosen for this result is particularly beneficial. An emissivity of 0.8 almost doubles the wavefront error.

The result might look contradictory: the SiC is well-known to be a robust material, not sensitive to thermal load. This is true only when considering the deformation model: for a given delta-T, the SiC is 6 times less deformable than Aluminum. But here the model also include a radiative thermal model. And SiC is 80 times less conductive than Aluminum; It means that Aluminum uniformizes 80 times more a thermal gradient than SiC. The two effects combined make the SiC more deformed when exposed without protection to the external heat sources.

Another step of validation was conducted in collaboration with Johan Petit, working at the Département Matériaux et Structure (DMAS) at ONERA. With the same inputs as the Excel model, they computed a thermal analysis with COMSOL. It gives a thermal gradient along the thickness of 0.984e-4K when the eight nodes Excel model gives 0.849e-4K. It validates the model with an uncertainty of 1.3e-5K, which seems satisfactory for our purpose.

3. STOP MODEL RESULTS

The final result expected from the STOP model in the analysis of the wavefront deformation during an orbit around the Earth. The time has been added in the model. The equation now becomes Equation 3, including the left term with temperature as a function of time, and the forcing terms on the right side also depending on time. As the petal orientation varies with time, always facing the Earth but some time back-sun, or edge-sun, a complete 3 dimensioned model with 8 nodes is necessary. This model has been developed in MATLAB, using an iterative solver. The input forcing terms have been estimated from the SimuSat software, providing the flux during an orbit on a given surface.

$$C\frac{dT_n(t)}{dt} = \Phi^n_{Sun}(t) + \Phi^n_{Earth\ IR}(t) + \Phi^n_{Albedo}(t) + \lambda\sum_{i=1}^{8} S_{ni}\ \frac{(T_n(t) - T_i(t))}{l_{ni}} - \sigma\epsilon S T_n^4(t)$$

Equation 3: heat balance equation, including time. In practice, all the terms are now depending on time.

Figure 6 shows the temperature gradient along the width of the petal, during a sequence of 15 orbits at summer solstice. This sequence duration covers a complete rotation of the satellite around the Earth and coming back at the nadir of its starting point.

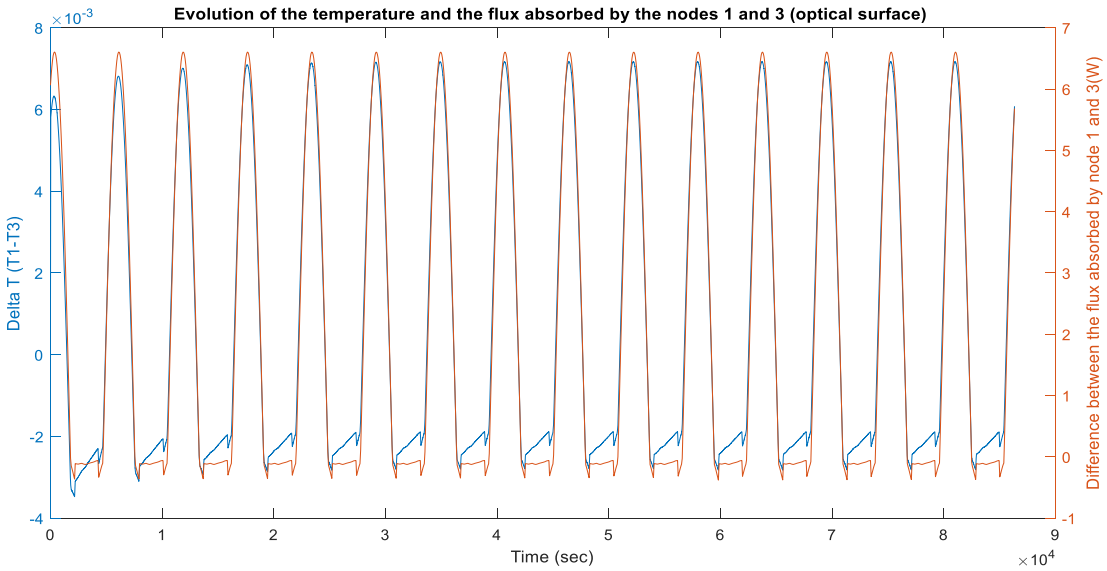

Figure 6: the difference of temperature between the two opposite faces of the petal are plotted (blue solid line) with respect to time. A period of 24h is considered here. At an orbit of 567km, this corresponds to 15 orbits. The temperature difference reaches 0.01K between maximum and minimum point. The maximum is reached for Earth-Satellite-Sun configuration. The minimum with Satellite-Earth-Sun configuration.

It shows that the temperature difference spans over 10mK (from +8mK in Sun-Satellite-Earth to -2mK for Sun-Earth-Satellite configuration) for this aluminium test case. In this test, we have chosen an emissivity of 0.8 for the non-polished surfaces. This evolution shows that in this configuration, the thermal distribution has just the time to establish close to the equilibrium.

The full temporal model is used to estimate the wavefront aberration generated along the orbit. The Figure 7 shows that Silicon Carbide, Titanium, Silicon nitride are out of specifications. Aluminum is just at the maximum acceptable level. In this case, we used a less optimistic value of 0.8 for emissivity for the non-polished surfaces.

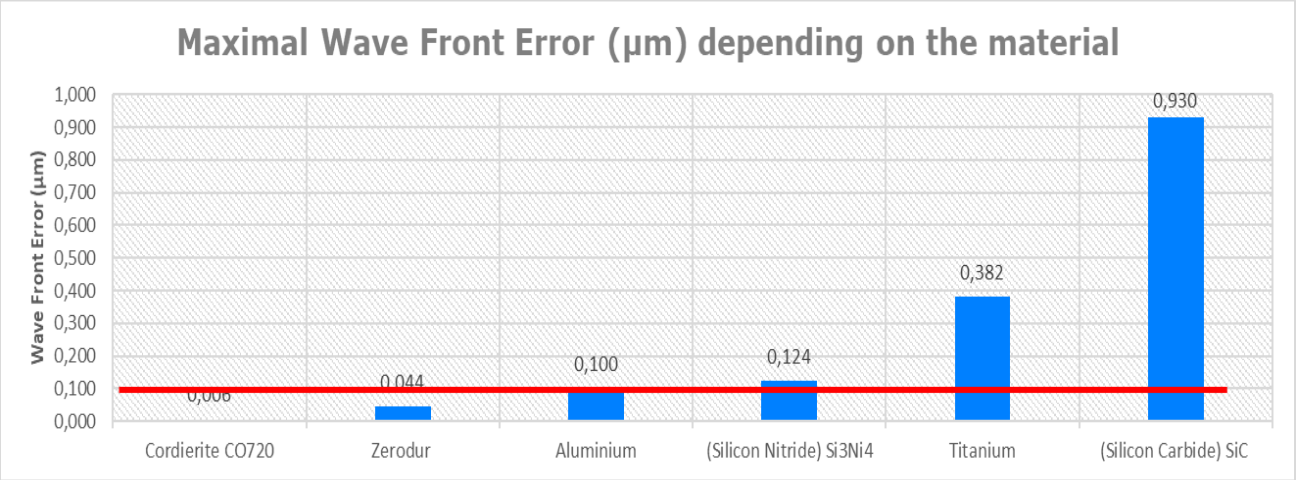

Figure 7: Wavefront aberration due to bending effect, during an orbit. The red solid line reminds the maximum acceptable value. Aluminum is right at the limit.

The analysis performed in this work show us the strong importance of the material for the final performance of the optical system. Aluminum, which is a good candidate for its simplicity to polish and its low cost, looks to be a good candidate, just at the limit though in this 10cm petal case.

4. CONCLUSION / PERSPECTIVES

We have presented in this paper a STOP model able to predict the deformation of the petal of a deployable telescope for CubeSat. The analysis, quite complete, includes the geometry of the petal, of the orbit, of the main heating sources (Sun, Earth, and space), as well as the material characteristics (conductivity, emissivity). The temporal evolution of each of these parameters is accounted for as well, and produces the final aberration generated by the heat environment of the satellite.

The analysis, although giving quantitative results, mainly helped us to understand the physical behaviour of the system. The conclusion nonetheless shows that Aluminum can be a good candidate to limit the impact of high order aberrations inside a petal.

The work performed thanks to this STOP model puts new constraints on the aberration measurement aspect. On top of the piston-tip-tilt modes expected to evolve, the high order modes as the bending of the petal might have to be measured as well, at least to deliver the PSF of the optical system to the final user. The work presented in [4] shows a first try on the estimation of the piston-tip-tilt modes and has to prove robustness to this high order modes.

The presence of these high order aberrations can however be post-corrected in the image, by taking into account the PSF in a deconvolution process.

5. ACKNOWLEDGEMENT

This work received support from ASHRA (Action Specifique Haute Résolution Angulaire), from INSU and CNES French national grant, for the collaboration between UK-ATC, LAM, ONERA and FeUP.
This work received support from ANR-WOLF (Principal Investigator Thierry Fusco) for J.-F. Sauvage travels.

[1] Schwartz, N., et al., “Laboratory demonstration of an active optics system for high-resolution deployable CubeSat,” in 4S Symposium, vol. 1, pp. 1–15 (2018).

[2] Sauvage, J.-F., et al. “AZIMOV: First error budget of a deployable CubeSat telescope,” Space Telescopes and Instrumentation 2020: Ultraviolet to Gamma Ray. Vol. 11444. International Society for Optics and Photonics, 2020.
[3] Schwartz, N., et al., “A segmented deployable primary mirror for earth observation from a CubeSat platform,” in Proc. AIAA/USU Conf. Small Satellite, vol. SSC16, p. SSC16–WK–23 (2016).
[4] Dumont, M., et al. “Deep learning for space-borne focal plane wavefront sensing,” Space Telescopes and Instrumentation 2022: Optical, Infrared, and Millimeter Wave, Proc. SPIE 12180, 12180-236 (2022).
[5] Noah Schwartz et al, 6U CubeSat deployable telescope for Earth Observation and Astronomical optical imaging, SPIE 2022